

hep-ph/0312024  
 ANL-HEP-PR-03-104  
 FERMILAB-Pub-03/378-T  
 RM3-TH/03-17  
 ILL-(TH)-03-10  
 NSF-KITP-03-98

February 8, 2020

## Associated Production of a $Z$ Boson and a Single Heavy-Quark Jet

**J. Campbell<sup>1</sup>, R. K. Ellis<sup>2</sup>, F. Maltoni<sup>3</sup>, and S. Willenbrock<sup>4,5</sup>**

<sup>1</sup>High Energy Physics Division, Argonne National Laboratory  
 Argonne, IL 60439

<sup>2</sup>Theoretical Physics Department, Fermi National Accelerator Laboratory  
 P. O. Box 500, Batavia, IL 60510

<sup>3</sup>Centro Studi e Ricerche “Enrico Fermi”  
 via Panisperna 89/A, 00184 Rome, Italy <sup>1</sup>

<sup>4</sup>Department of Physics, University of Illinois at Urbana-Champaign  
 1110 West Green Street, Urbana, IL 61801

<sup>5</sup>Kavli Institute for Theoretical Physics, University of California  
 Santa Barbara, CA 93106

### Abstract

The leading-order process for the production of a  $Z$  boson and a heavy-quark jet at hadron colliders is  $gQ \rightarrow ZQ$  ( $Q = c, b$ ). We calculate this cross section at next-to-leading order at the Tevatron and the LHC, and compare it with other sources of  $ZQ$  events. This process is a background to new physics, and can be used to measure the heavy-quark distribution function.

---

<sup>1</sup>Mail address: Dipartimento di Fisica, Terza Università di Roma, via della Vasca Navale 84, 00146 Rome, Italy

# 1 Introduction

Many signals for new physics at hadron colliders involve electroweak gauge bosons ( $W^\pm, Z, \gamma$ ) and jets containing heavy quarks ( $c, b$ ). The prime example is  $W + 4$  jets, with one or more jets containing a  $b$  tag, which led to the discovery of the top quark [1, 2, 3]. Other examples include signals for the Higgs boson and the superpartners of the known particles [4, 5]. It is therefore crucial to understand the standard-model background from the production of electroweak bosons and heavy-quark jets with good accuracy.

The simplest processes of this type are the production of a single electroweak gauge boson and one heavy-quark jet. In the case of the  $W$  boson, the leading-order process is  $gs \rightarrow W^- c$  [6], which has been calculated at next-to-leading order (with  $m_c$  nonzero) [7]. For a photon, the leading-order process is  $gQ \rightarrow \gamma Q$  ( $Q = c, b$ ), which has also been calculated at next-to-leading order (with  $m_Q = 0$ ) [8, 9]. In this paper we consider the analogous leading-order process for the  $Z$  boson,  $gQ \rightarrow ZQ$ , shown in Fig. 1, which we calculate at next-to-leading order (with  $m_Q = 0$ ).

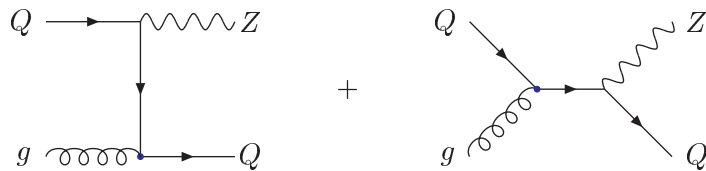


Figure 1: Associated production of a  $Z$  boson and a single high- $p_T$  heavy quark ( $Q = c, b$ ).

An alternative calculational scheme is to regard  $gg \rightarrow ZQ\bar{Q}$  as the leading-order process (with  $m_Q$  nonzero), and to allow one heavy quark to be emitted collinear to the beam, yielding a  $ZQ$  final state. This approach has two drawbacks. First, the expansion parameter of this calculation is  $\alpha_S \ln(M_Z/m_Q)$  rather than  $\alpha_S$ , so perturbation theory is less convergent. Using a heavy-quark distribution function sums these collinear logarithms to all orders, resulting in a perturbative expansion in  $\alpha_S$  and  $1/\ln(M_Z/m_Q)$  [10, 11, 12]. Second, it is much more difficult to obtain the next-to-leading-order correction to  $gg \rightarrow ZQ\bar{Q}$  than to  $gQ \rightarrow ZQ$ , both because there is one more particle in the final state, and because the heavy-quark mass must be maintained in the calculation of  $gg \rightarrow ZQ\bar{Q}$  to regulate the collinear region (one may set  $m_Q = 0$  in  $gQ \rightarrow ZQ$ , provided that the heavy-quark transverse momentum is much larger than its mass). At present,  $gg \rightarrow ZQ\bar{Q}$  is known at next-to-leading order only for  $m_Q = 0$  [13, 14, 15]. In contrast, the next-to-leading-order calculation of  $gQ \rightarrow ZQ$  (with  $m_Q = 0$ ) that we perform in this paper is sufficiently straightforward that the next-to-next-to-leading-order calculation may be available in the foreseeable future [16].

The process  $gQ \rightarrow ZQ$  is a background to  $gb \rightarrow hb$ , where the  $Z$  boson and the Higgs boson decay to the same final state ( $b\bar{b}, \tau^+\tau^-$ , or  $\mu^+\mu^-$ ) [17, 18, 19]. In addition,  $gQ \rightarrow ZQ$  could potentially be used to measure the  $Q$  distribution function. The  $b$  distribution function is needed for the above-mentioned Higgs-production process as well as for inclusive Higgs production,  $b\bar{b} \rightarrow h$  [20, 21, 22]. It is also needed for the single-top production processes

$qb \rightarrow q't$  [12, 23] and  $gb \rightarrow W^-t$  [24, 25] and the charged-Higgs production process  $gb \rightarrow H^-t$  [26, 27, 28]. At present, the  $b$  distribution function is derived perturbatively from the gluon distribution function [10, 11, 29] and there is no direct measurement of it. The process  $gQ \rightarrow \gamma Q$  is much more sensitive to the charm distribution function than to that of bottom, due to the greater electric charge of the charm quark [30, 31].

Another source of  $ZQ$  events is  $q\bar{q} \rightarrow ZQ\bar{Q}$ , shown in Fig. 2, where either one  $Q$  is missed, or the two  $Q$ 's coalesce into a single jet. We show that this process is much more significant at the Tevatron than at the LHC, since light-quark distribution functions are relatively more important at large values of Bjorken  $x$ . This calculation is carried out at leading order with a non-zero  $Q$  mass.

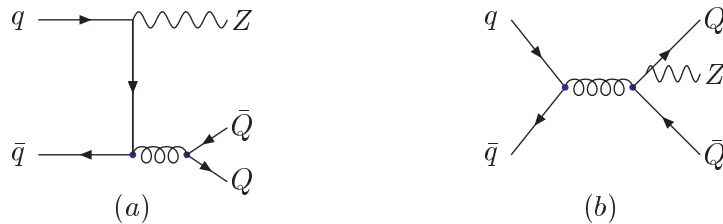


Figure 2: Representative Feynman diagrams for  $q\bar{q} \rightarrow ZQ\bar{Q}$ . The  $Z$  boson may be radiated off (a) the initial-state quarks or (b) the final-state quarks.

In addition, we also calculate  $Zj$  production at next-to-leading order, where  $j$  denotes a light-quark or gluon jet, as shown in Fig. 3 [32, 33, 34]. Using a silicon vertex detector to tag heavy quarks, the probability that such a jet fakes a heavy-quark jet is around 1%. Taking this probability into account, we show that this source of fake  $ZQ$  events is comparable to genuine  $ZQ$  events at the Tevatron, but is relatively less important at the LHC.



Figure 3: Representative Feynman diagrams for  $Zj$  production via (a)  $gq \rightarrow Zq$  and (b)  $q\bar{q} \rightarrow Zg$ .

All of the above processes can also lead to final states with two jets, with varying numbers of heavy quarks. For completeness, we also calculate these cross sections (at leading order). When combined with the next-to-leading-order cross section for  $ZQ$ , one obtains the inclusive cross section for  $Z$  plus at least one heavy-quark jet (at next-to-leading order).

The next-to-leading-order calculations in this paper were performed with the Monte-Carlo code MCFM [35]. The leading-order calculations were performed both with this code and with MadEvent [36].

## 2 $gQ \rightarrow ZQ$ at NLO

The next-to-leading-order (NLO) calculation of  $gQ \rightarrow ZQ$  parallels our NLO calculation of  $gb \rightarrow hb$  [19], and we refer the reader to that work for a detailed discussion of the calculational scheme. The contributing subprocesses are

- $gQ \rightarrow ZQ$  (one loop)
- $qQ \rightarrow ZQq$
- $gQ \rightarrow ZQg$
- $gg \rightarrow ZQ\bar{Q}$

The subprocess  $q\bar{q} \rightarrow ZQ\bar{Q}$  is considered separately in the following section, and is not regarded as a correction to  $gQ \rightarrow ZQ$ .

We work in the simplified ACOT scheme [10, 11], which allows one to neglect the  $Q$  mass throughout. This is a good approximation, and simplifies the calculation. The error made by this approximation is proportional to  $1/\ln(M_Z/m_Q) \times m_Q^2/p_T^2$  [19]. We use the dipole-subtraction method [37] as formulated in Ref. [38] to isolate and subtract collinear divergences.

In our NLO calculation of  $gQ \rightarrow ZQ$ , we demand one and only one jet with transverse momentum  $p_T > 15$  GeV within a rapidity range  $|\eta| < 2$  at the Fermilab Tevatron. This jet must contain a heavy quark. At the CERN Large Hadron Collider (LHC), the heavy-quark jet must have  $p_T > 15$  GeV and  $|\eta| < 2.5$ .

If two partons lie within a cone of radius  $\Delta R < 0.7$ , we merge them into a single jet with four-momentum equal to the sum of the two partons' four-momenta. This is done before the cuts described above are applied to the jets. The NLO process  $gg \rightarrow ZQ\bar{Q}$  yields two heavy quarks in the final state. If they are merged into a single jet, we record it as a double-heavy-quark jet. This is only about 1% of the  $ZQ$  cross section.

Similarly, the NLO process  $QQ' \rightarrow QQ'Z$ , and processes related by crossing, yield two heavy quarks in the final state. However, these processes amount to a correction of less than 1%, so we neglect them [19].

We list in the first column of Tables 1 and 2 the LO (in parentheses) and NLO cross sections for  $gb \rightarrow Zb$  and  $gc \rightarrow Zc$  at the Tevatron and the LHC. The  $Zc$  cross section exceeds that of  $Zb$  by 70% at the Tevatron and 35% at the LHC because the charm distribution function is larger than that of bottom. This is partially compensated by the fact that the  $Z$  has stronger coupling to bottom than to charm. The ratio of the  $Zb$  and  $Zc$  partonic cross sections is proportional to

$$\frac{V_b^2 + A_b^2}{V_c^2 + A_c^2} = \frac{1 + (1 - \frac{4}{3} \sin^2 \theta_W)^2}{1 + (1 - \frac{8}{3} \sin^2 \theta_W)^2} \approx 13/10 .$$

More importantly, a silicon vertex detector (SVX) can tag a  $b$  jet with an efficiency around 60%, and a  $c$  jet with an efficiency of about 15%. Thus the majority of  $ZQ$  events tagged with an SVX come from  $Zb$ .

The NLO processes that contribute to  $ZQ$  also give rise to final states with more than one jet, and we list these cross sections in the remaining columns. These events are grouped in three classes. The second column, labeled  $Z(Q\bar{Q})$ , corresponds to events with a single jet that contains two heavy quarks. As mentioned earlier, this is only about 1% of the  $ZQ$  cross section. The third column, labeled  $ZQj$ , corresponds to events with two jets, one of which contains a heavy quark. This is about 1/5 of the  $ZQ$  cross section at the Tevatron, and about 1/2 at the LHC (for  $p_T > 15$  GeV). The fourth column, labeled  $ZQ\bar{Q}$ , corresponds to events with two jets, both of which contain heavy quarks. This is significantly less than  $ZQj$ . The  $ZQ\bar{Q}$  events arise from the NLO process  $gg \rightarrow ZQ\bar{Q}$  (as do the  $Z(Q\bar{Q})$  events). The final column sums these various processes, to give the inclusive cross section for  $Z$  plus at least one heavy-quark jet at next-to-leading order.

We show in Figs. 4–7 the scale dependence of the inclusive cross section for  $Zb$  and  $Zc$  production at the Tevatron and the LHC at leading order (LO) and next-to-leading order (NLO). The dependence on the renormalization and factorization scales are shown separately. Both scale dependencies are reduced at NLO in comparison with LO. We use  $\mu_R = M_Z$ ,  $\mu_F = M_Z$  as our default value of the renormalization and factorization scales.

We also estimate the uncertainty in the NLO inclusive cross section. The first uncertainty is due to varying the renormalization scale between half and twice its default value of  $\mu_R = M_Z$ . The second uncertainty, obtained in the same manner, is due to the factorization scale. The third uncertainty is from the parton distribution functions [29]. There is also an additional uncertainty of 4% due to  $\delta\alpha_S(M_Z) = 0.002$ . [39]

We show in Figs. 8–9 the transverse-momentum distributions of both the  $Z$  and the highest- $p_T$   $b$  jet at the Tevatron and the LHC. At leading order these distributions are identical, since the  $Z$  recoils against the  $b$  jet. At next-to-leading order the distributions for the inclusive cross section are slightly different, since the  $Z$  can recoil against two jets. The distributions for  $Zc$  production are qualitatively similar.

### 3 $q\bar{q} \rightarrow ZQ\bar{Q}$ at LO

Another contribution to  $ZQ$  production comes from  $q\bar{q} \rightarrow ZQ\bar{Q}$  ( $q = u, d, s$ ), shown in Fig. 2, where one  $Q$  is outside the coverage of the detector. The dominant contribution to the cross section comes from diagrams in which the  $Z$  is radiated from the initial-state quarks while the heavy quarks arise from gluon splitting, as shown in Fig. 2(a). We maintain the heavy-quark mass throughout the calculation in order to regulate the singularity that would arise from a gluon splitting to massless collinear quarks. Although the NLO cross section for this process with massless quarks is available [13, 14, 15], the cross section with massive quarks is known only at LO.

The LO cross section for  $ZQ$  production via  $q\bar{q} \rightarrow ZQ\bar{Q}$  is given in the first column of Tables 1 and 2. At the Tevatron, the cross section is about 1/3 of  $gQ \rightarrow ZQ$ . At the LHC, the contribution from  $q\bar{q} \rightarrow ZQ\bar{Q}$  is relatively much less, only about 1/30 of  $gQ \rightarrow ZQ$ . This reflects the fact that this process is initiated by a  $q\bar{q}$  collision. At the Tevatron, where the typical values of Bjorken  $x$  are relatively large, the valence quark distribution functions are significant. In contrast, the typical values of  $x$  are relatively small at the LHC, so the valence quark distribution functions are less important.

Table 1: Cross sections (pb) for  $Z$ -boson production in association with heavy-quark jets at the Tevatron ( $\sqrt{s} = 1.96$  TeV  $p\bar{p}$ ). A jet lies in the range  $p_T > 15$  GeV and  $|\eta| < 2$ . Two final-state partons are merged into a single jet if  $R_{jj} < 0.7$ . No branching ratios or tagging efficiencies are included. The labels on the columns have the following meaning:  $ZQ$  = exactly one jet, which contains a heavy quark;  $Z(Q\bar{Q})$  = exactly one jet, which contains two heavy quarks;  $ZQj$  = exactly two jets, one of which contains a heavy quark;  $ZQ\bar{Q}$  = exactly two jets, both of which contain a heavy quark. For the last set of processes, the labels mean:  $Zj$  = exactly one jet, which does not contain a heavy quark;  $Zjj$  = exactly two jets, neither of which contain a heavy quark. For  $ZQ$  and  $Zj$ , both the leading-order (in parentheses) and next-to-leading-order cross sections are given. The last column is the next-to-leading-order inclusive cross section, which is the sum of four previous columns. The CTEQ6M parton distribution functions are used throughout, except for the LO cross sections in parentheses, where CTEQ6L1 is used [29]. The factorization and renormalization scales are chosen as  $\mu_F = \mu_R = M_Z$ . The uncertainties are from the variation of the renormalization scale, the factorization scale, and the parton distribution functions, respectively.

Cross sections (pb)	Tevatron				
	$ZQ$	$Z(Q\bar{Q})$	$ZQj$	$ZQ\bar{Q}$	$ZQ$ inclusive
$gb \rightarrow Zb$	(8.23)	10.4	0.169	2.19	0.631
$q\bar{q} \rightarrow Zb\bar{b}$		3.32	1.92	—	1.59
$gc \rightarrow Zc$	(11.3)	16.5	0.130	3.22	0.49
$q\bar{q} \rightarrow Zc\bar{c}$		5.66	6.45	—	1.70
	$Zj$		$Zjj$		$Zj$ inclusive
$q\bar{q} \rightarrow Zg, gq \rightarrow Zq$	(876)		870		1010 $^{+44}_{-40}$ $^{+9}_{-2}$ $^{+7}_{-12}$

The second column in Tables 1 and 2 lists the contribution from  $q\bar{q} \rightarrow ZQ\bar{Q}$  when the  $Q$  and  $\bar{Q}$  merge into a single jet. This is comparable in size to the contribution of this process to  $ZQ$  production. This is due to the aforementioned enhancement that arises when the heavy quarks are collinear. This process is the dominant source of events where the  $Z$  is accompanied by a single jet that contains two heavy quarks.

The last column gives the contribution of  $q\bar{q} \rightarrow ZQ\bar{Q}$  when both jets are within the coverage of the detector. The  $Zb\bar{b}$  cross section is about 1/2 of the  $Zb$  cross section from this process at both machines, and the  $Zc\bar{c}$  cross section is about 1/3 of the  $Zc$  cross section. This is in contrast with the  $gQ \rightarrow ZQ$  process, where the  $ZQ\bar{Q}$  final state (that arises at NLO) is much less than  $ZQ$ .

Table 2: Same as Table 1, except at the LHC ( $\sqrt{s} = 14$  TeV  $pp$ ). A jet lies in the range  $p_T > 15$  GeV and  $|\eta| < 2.5$ .

Cross sections (pb)	LHC				
	$ZQ$	$Z(Q\bar{Q})$	$ZQj$	$ZQ\bar{Q}$	$ZQ$ inclusive
$gb \rightarrow Zb$	(826) 649	11.3	304	78.1	$1040^{+70+70+30}_{-60-100-50}$
$q\bar{q} \rightarrow Zb\bar{b}$	24.3	13.5	–	11.4	49.2
$gc \rightarrow Zc$	(989) 921	8.8	396	61.5	$1390 \pm 100^{+60+40}_{-70-80}$
$q\bar{q} \rightarrow Zc\bar{c}$	36.7	41.7	–	11.3	89.7
	$Zj$		$Zjj$		$Zj$ inclusive
$q\bar{q} \rightarrow Zg, gq \rightarrow Zq$	(13500) 11600		4270		$15870^{+900+60+300}_{-600-300-500}$

## 4 $q\bar{q} \rightarrow Zq, gq \rightarrow Zq$ at NLO

A light-quark or gluon jet can fake a heavy-quark jet. With a silicon vertex detector, the mistagging rate is typically around 1%. Since the cross section for  $Zj$  production is much greater than that for  $ZQ$ , it is potentially a large source of fake  $ZQ$  events.

We list in Tables 1 and 2 the LO (in parentheses) and NLO cross sections for  $Zj$  production. The LO processes are  $q\bar{q} \rightarrow Zg$  ( $q = u, d, s, c, b$ ) and  $gq \rightarrow Zq$  ( $q = u, d, s$ ), as shown in Fig. 3. The NLO processes also contribute to the  $Zjj$  final state, and we list that cross section in the Tables as well. The  $Zj$  cross section is almost two orders of magnitude greater than that of  $gQ \rightarrow ZQ$  at the Tevatron. Taking into account the 1% mistagging rate, we see that  $Zj$  is a significant source of fake  $ZQ$  events at the Tevatron. In contrast, at the LHC the  $Zj$  cross section is not nearly as significant. Thus there will be relatively fewer mistagged events at the LHC. Qualitatively similar results are obtained for the ratio of  $Zjj$  to  $ZQj$ .

## 5 Conclusions

The dominant contribution to  $Zb$  production is  $gb \rightarrow Zb$ . At the Tevatron,  $q\bar{q} \rightarrow Zb\bar{b}$  also makes a significant contribution. Combining these two contributions, the total inclusive cross section for  $Zb$  production at the Tevatron is about 20 pb. Thus there are about 2000 inclusive  $Zb$  events produced within the coverage of the detector at the Tevatron for every 100 pb<sup>-1</sup> of integrated luminosity delivered. The cleanest decay mode of the  $Z$  boson is to leptons ( $\ell = e, \mu$ ), with a branching ratio of 6.7%. Including a  $b$ -tagging efficiency of 60% yields about 80 tagged ( $Z \rightarrow \ell^+\ell^-$ ) $b$  events for every 100 pb<sup>-1</sup>. There are slightly more tagged events when one accounts for the fact that some events contain two heavy quarks, either within the same jet or in separate jets. With data sets between 4000 and 8000 pb<sup>-1</sup>

expected in Run II at the Tevatron, there will be between 3200 and 6400 tagged ( $Z \rightarrow \ell^+\ell^-$ ) $b$  events.

At the LHC, the contribution from  $q\bar{q} \rightarrow Zb\bar{b}$  is much less significant, so most of the cross section comes from  $gb \rightarrow Zb$ . The total inclusive cross section for  $Zb$  production is about 1090 pb, a factor of about 50 larger than at the Tevatron. Thus there will be an enormous number of  $Zb$  events at the LHC.

The total inclusive cross section for  $Zc$  production at the Tevatron is about 70% greater than that of  $Zb$ , while at the LHC,  $Zc$  is about 35% greater than  $Zb$ . However, the SVX tagging efficiency for charm is about 1/4 of the  $b$ -tagging efficiency, so there will be fewer tagged  $Zc$  events than tagged  $Zb$  events. In contrast, the number of  $\gamma c$  events far outweighs the number of  $\gamma b$  events at both machines, since charm has twice the electric charge of bottom and the charm distribution function is larger than that of bottom. Even taking the greater tagging efficiency of bottom into account, the number of tagged  $\gamma c$  events is larger than the number of tagged  $\gamma b$  events [30, 31].

$Zj$  events, where the jet is mistagged as a heavy quark, are a significant source of fake  $ZQ$  events at the Tevatron, but much less so at the LHC. Thus a larger fraction of the tagged  $ZQ$  events at the LHC will be from genuine heavy-quark production. For this reason, and also due to the relatively smaller contribution from  $q\bar{q} \rightarrow ZQ\bar{Q}$ , the LHC provides a cleaner environment for the extraction of the heavy-quark distribution functions via  $gQ \rightarrow ZQ$ .

In addition to the decay  $Z \rightarrow \ell^+\ell^-$ , there will be many  $Z \rightarrow \nu\bar{\nu}$  events ( $BR = 20\%$ ), which will yield heavy-quark monojets. This will also yield dijet events with large missing transverse momentum, with one or both jets containing heavy quarks.

Regardless of the  $Z$  decay mode, the majority of  $Z + 2$  jet events with a single heavy-quark tag at the LHC come from  $ZQj$ , not  $ZQ\bar{Q}$ . At the Tevatron, where  $q\bar{q} \rightarrow ZQ\bar{Q}$  is relatively more important, the  $ZQj$  and  $ZQ\bar{Q}$  final states are comparable in size.

## Acknowledgments

We are grateful for conversations and correspondence with L. Christofek, T. Junk, T. Liss, K. Pitts, D. Stuart, M. Whalley, and J. Womersley. F. M. warmly thanks the Department of Physics of the “Terza Università di Roma” for the kind hospitality and support. S. W. thanks the Aspen Center for Physics for hospitality. This work was supported in part by the U. S. Department of Energy under contracts Nos. DE-AC02-76CH03000 and DE-FG02-91ER40677 and by the National Science Foundation under Grant No. PHY99-07949.

## References

- [1] F. Abe *et al.* [CDF Collaboration], Phys. Rev. Lett. **74**, 2626 (1995) [arXiv:hep-ex/9503002].
- [2] S. Abachi *et al.* [D0 Collaboration], Phys. Rev. Lett. **74**, 2632 (1995) [arXiv:hep-ex/9503003].

- [3] D. Acosta *et al.* [CDF Collaboration], Phys. Rev. D **65**, 052007 (2002) [arXiv:hep-ex/0109012].
- [4] M. Carena and J. Lykken, “Physics at Run II: Supersymmetry/Higgs Workshop,” FERMILAB-PUB-00-349 *Prepared for Physics at Run II: Workshop on Supersymmetry / Higgs: 1st General Meeting, Batavia, Illinois, 14-16 May 1998*.
- [5] ATLAS Collaboration, Technical Design Report, CERN-LHCC-99-15.
- [6] U. Baur, F. Halzen, S. Keller, M. L. Mangano and K. Riesselmann, Phys. Lett. B **318**, 544 (1993) [arXiv:hep-ph/9308370].
- [7] W. T. Giele, S. Keller and E. Laenen, Phys. Lett. B **372**, 141 (1996) [arXiv:hep-ph/9511449].
- [8] E. L. Berger and L. E. Gordon, Phys. Rev. D **54**, 2279 (1996) [arXiv:hep-ph/9512343].
- [9] B. Bailey, E. L. Berger and L. E. Gordon, Phys. Rev. D **54**, 1896 (1996) [arXiv:hep-ph/9602373].
- [10] M. A. Aivazis, J. C. Collins, F. I. Olness and W. K. Tung, Phys. Rev. D **50**, 3102 (1994) [arXiv:hep-ph/9312319].
- [11] J. C. Collins, Phys. Rev. D **58**, 094002 (1998) [arXiv:hep-ph/9806259].
- [12] T. Stelzer, Z. Sullivan and S. Willenbrock, Phys. Rev. D **56**, 5919 (1997) [arXiv:hep-ph/9705398].
- [13] J. M. Campbell and R. K. Ellis, Phys. Rev. D **62**, 114012 (2000) [arXiv:hep-ph/0006304].
- [14] J. Campbell and R. K. Ellis, Phys. Rev. D **65**, 113007 (2002) [arXiv:hep-ph/0202176].
- [15] J. Campbell, R. K. Ellis and D. Rainwater, arXiv:hep-ph/0308195.
- [16] E. W. N. Glover, Nucl. Phys. Proc. Suppl. **116**, 3 (2003) [arXiv:hep-ph/0211412].
- [17] D. Choudhury, A. Datta and S. Raychaudhuri, arXiv:hep-ph/9809552.
- [18] C. S. Huang and S. H. Zhu, Phys. Rev. D **60**, 075012 (1999) [arXiv:hep-ph/9812201].
- [19] J. Campbell, R. K. Ellis, F. Maltoni and S. Willenbrock, Phys. Rev. D **67**, 095002 (2003) [arXiv:hep-ph/0204093].
- [20] D. Dicus, T. Stelzer, Z. Sullivan and S. Willenbrock, Phys. Rev. D **59**, 094016 (1999) [arXiv:hep-ph/9811492].
- [21] C. Balazs, H. J. He and C. P. Yuan, Phys. Rev. D **60**, 114001 (1999) [arXiv:hep-ph/9812263].
- [22] F. Maltoni, Z. Sullivan and S. Willenbrock, Phys. Rev. D **67**, 093005 (2003) [arXiv:hep-ph/0301033].

- [23] T. Stelzer, Z. Sullivan and S. Willenbrock, Phys. Rev. D **58**, 094021 (1998) [arXiv:hep-ph/9807340].
- [24] A. P. Heinonen, A. S. Belyaev and E. E. Boos, Phys. Rev. D **56**, 3114 (1997) [arXiv:hep-ph/9612424].
- [25] S. Zhu, Phys. Lett. B **524** (2002) 283 [Erratum-ibid. B **537** (2002) 351].
- [26] V. D. Barger, R. J. N. Phillips and D. P. Roy, Phys. Lett. B **324**, 236 (1994) [arXiv:hep-ph/9311372].
- [27] S. h. Zhu, Phys. Rev. D **67**, 075006 (2003) [arXiv:hep-ph/0112109].
- [28] T. Plehn, Phys. Rev. D **67**, 014018 (2003) [arXiv:hep-ph/0206121].
- [29] J. Pumplin, D. R. Stump, J. Huston, H. L. Lai, P. Nadolsky and W. K. Tung, JHEP **0207**, 012 (2002) [arXiv:hep-ph/0201195].
- [30] F. Abe *et al.* [CDF Collaboration], Phys. Rev. Lett. **83**, 3124 (1999) [arXiv:hep-ex/9810031].
- [31] T. Affolder *et al.* [CDF Collaboration], Phys. Rev. D **65**, 052006 (2002) [arXiv:hep-ex/0106012].
- [32] P. B. Arnold and M. H. Reno, Nucl. Phys. B **319**, 37 (1989) [Erratum-ibid. B **330**, 284 (1990)].
- [33] R. J. Gonsalves, J. Pawlowski and C. F. Wai, Phys. Rev. D **40**, 2245 (1989).
- [34] W. T. Giele, E. W. Glover and D. A. Kosower, Nucl. Phys. B **403**, 633 (1993) [arXiv:hep-ph/9302225].
- [35] R. K. Ellis *et al.* [QCD Tools Working Group Collaboration], arXiv:hep-ph/0011122.
- [36] F. Maltoni and T. Stelzer, JHEP **0302**, 027 (2003) [arXiv:hep-ph/0208156].
- [37] R. K. Ellis, D. A. Ross and A. E. Terrano, Nucl. Phys. B **178**, 421 (1981).
- [38] S. Catani and M. H. Seymour, Nucl. Phys. B **485**, 291 (1997) [Erratum-ibid. B **510**, 503 (1997)] [arXiv:hep-ph/9605323].
- [39] K. Hagiwara *et al.* [Particle Data Group Collaboration], Phys. Rev. D **66**, 010001 (2002).

$p\bar{p} \rightarrow Zb$  @ Tevatron

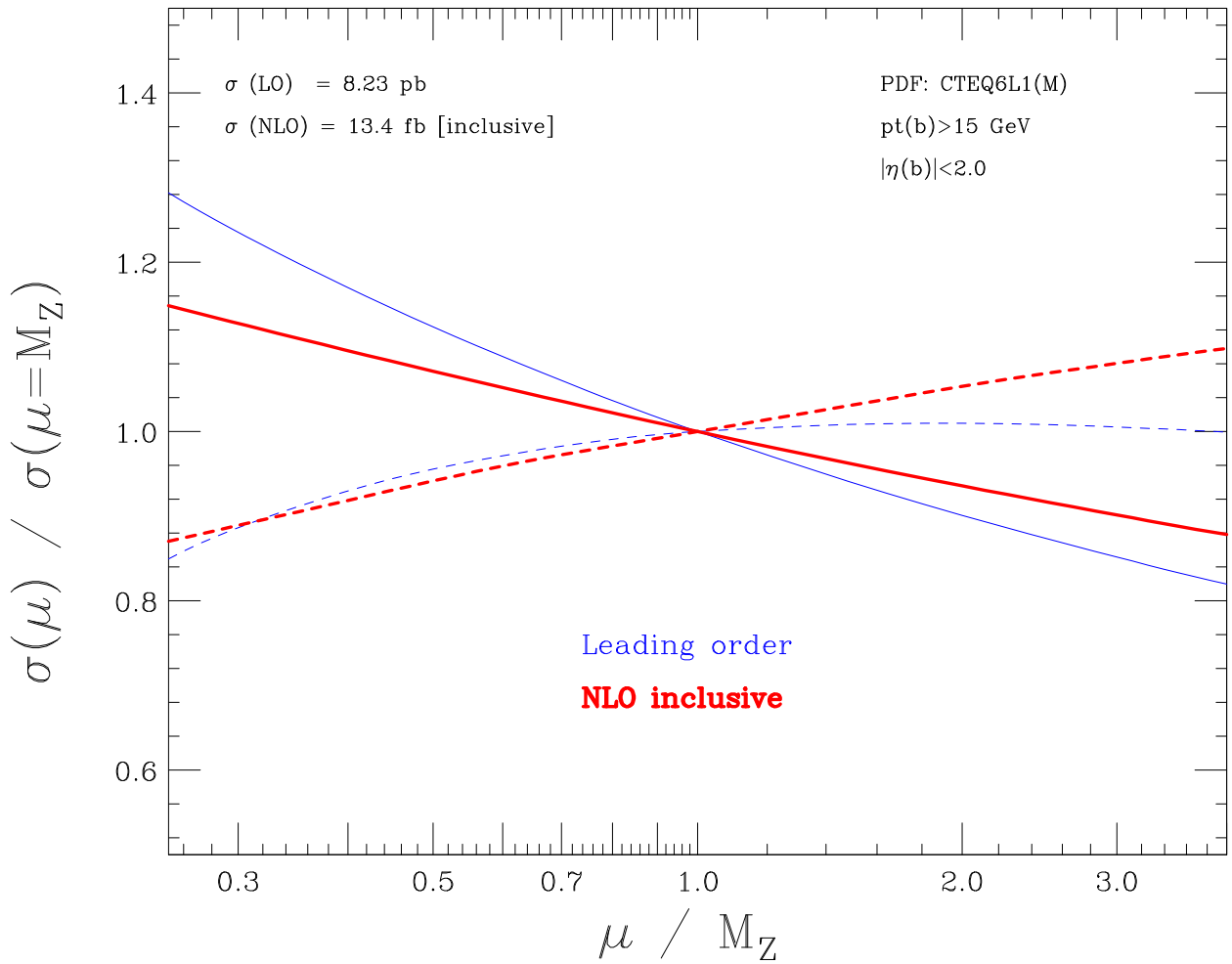


Figure 4: Cross section for  $gb \rightarrow Zb$  at the Tevatron *vs.* the renormalization scale (solid curves) and factorization scale (dashed curves). The ratio of the cross section at scale  $\mu$  to the cross section at scale  $\mu = M_Z$  is plotted *vs.* the ratio of the scales. The next-to-leading-order (NLO) inclusive cross section (bold) is less sensitive to the scales than the leading-order (LO) cross section (regular).

pp $\rightarrow$ Zb @ LHC

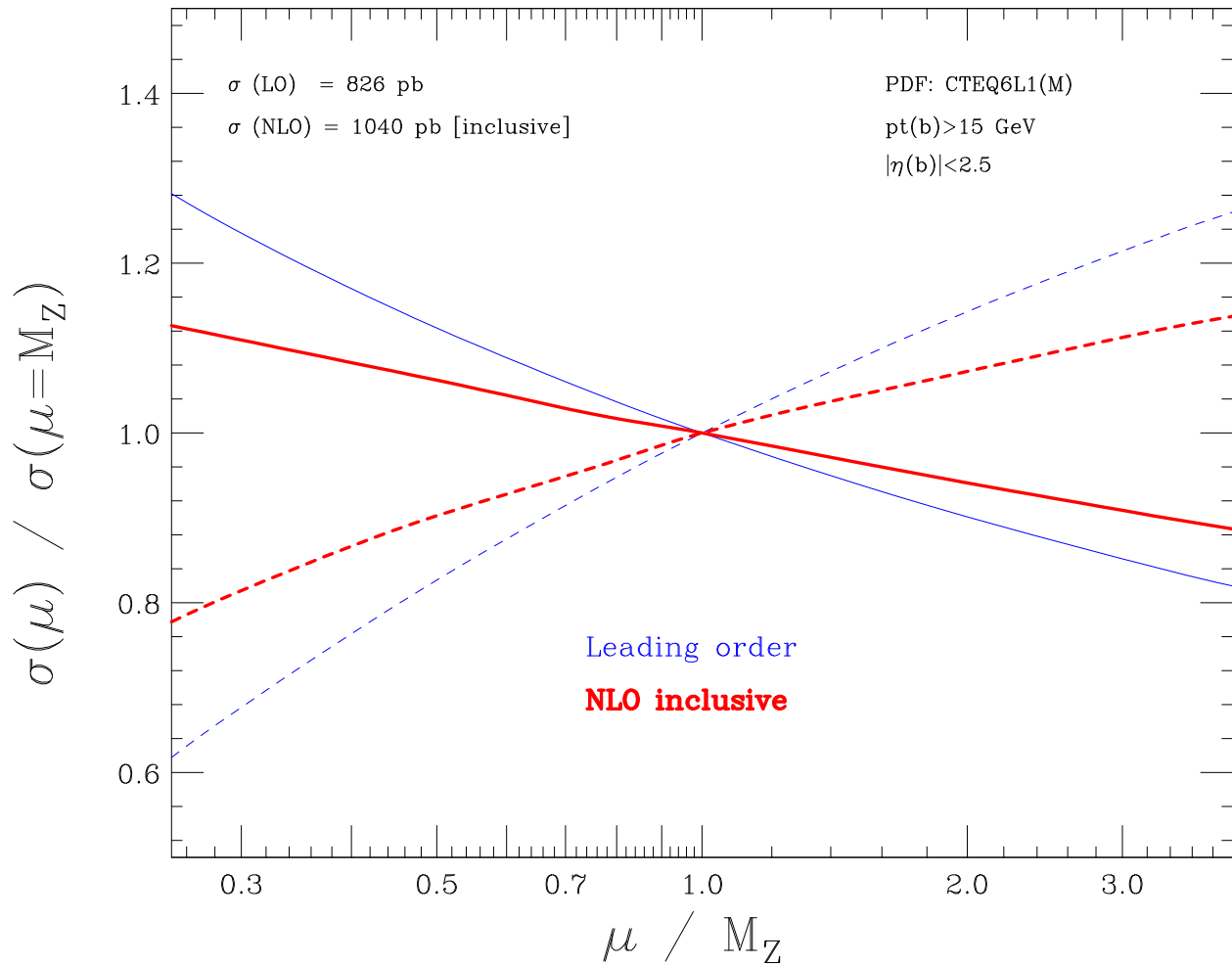


Figure 5: Same as Fig. 4, but at the LHC.

$p\bar{p} \rightarrow Zc$  @ Tevatron

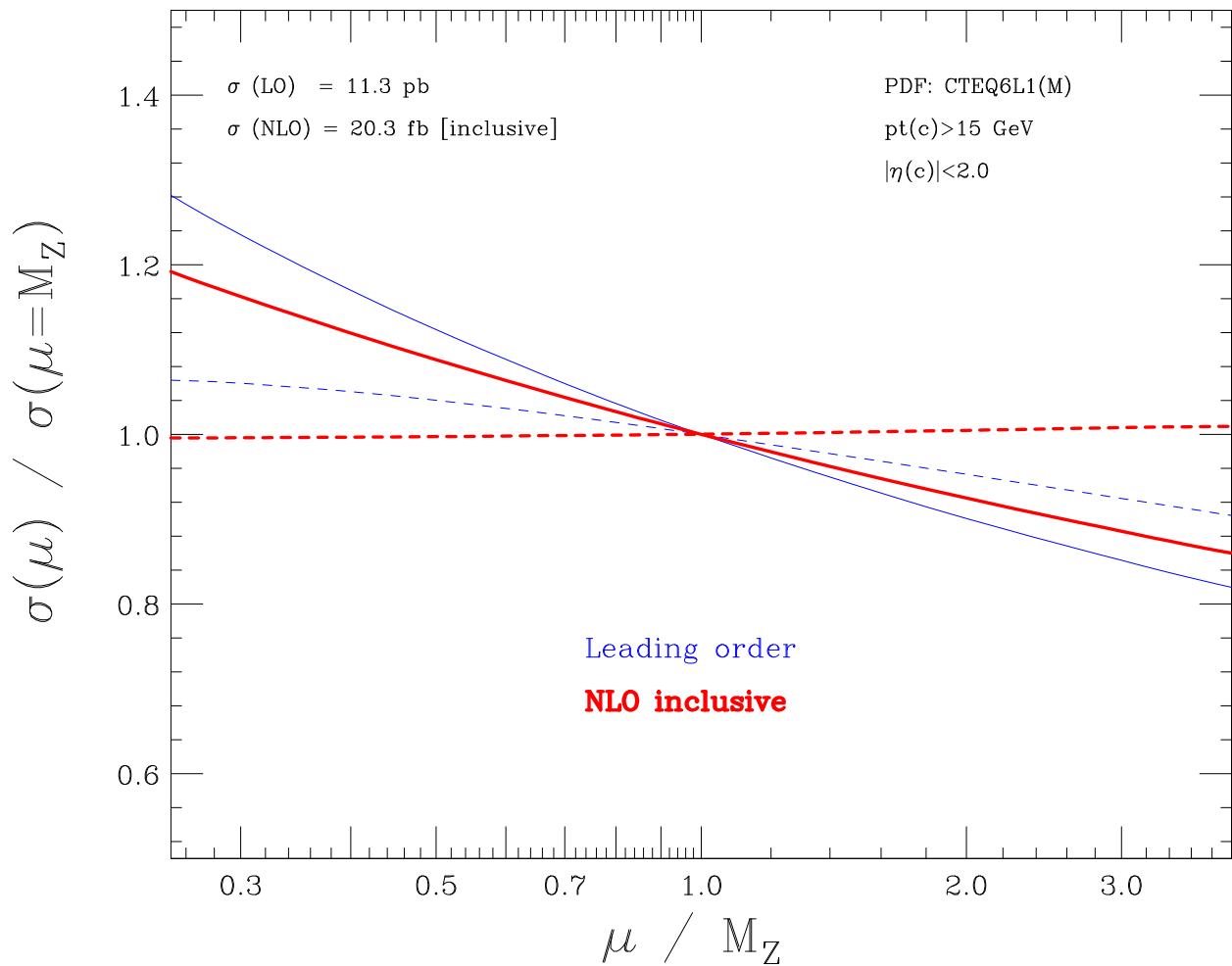


Figure 6: Same as Fig. 4, but for  $Zc$  production.

pp $\rightarrow$ Z<sub>C</sub> @ LHC

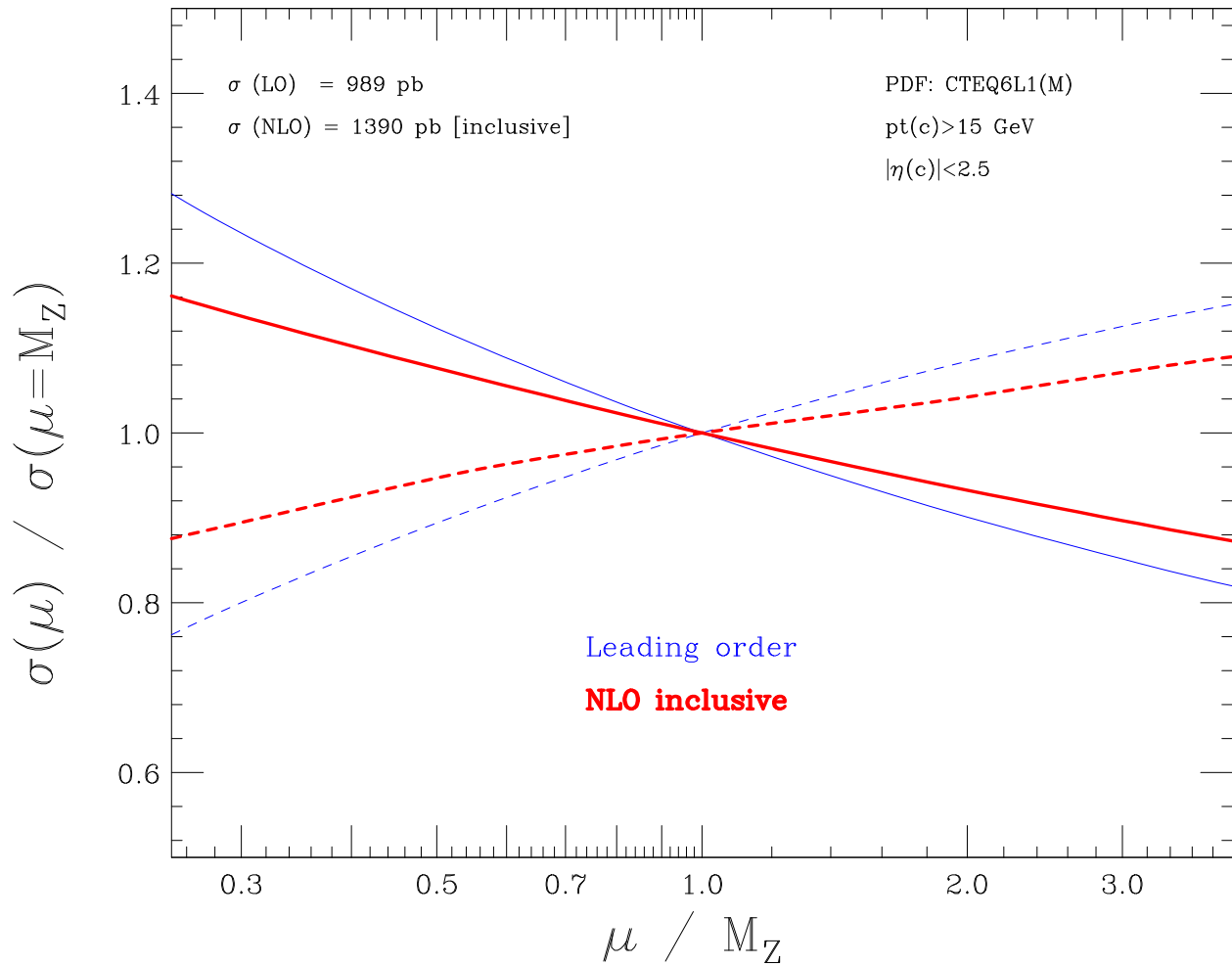


Figure 7: Same as Fig. 6, but at the LHC.

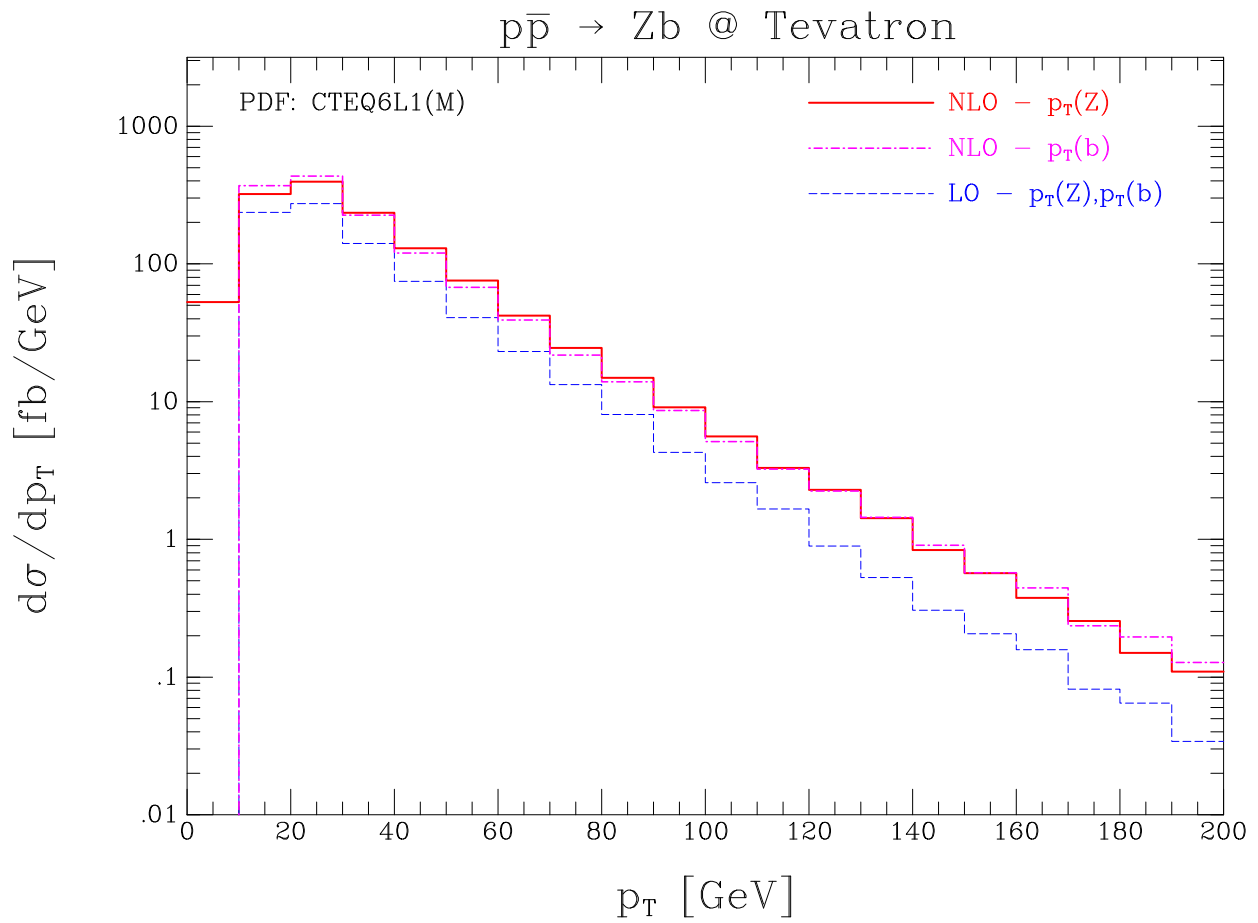


Figure 8: The transverse-momentum distribution of  $gb \rightarrow Zb$  at the Tevatron. Qualitatively similar results are obtained for  $gc \rightarrow Zc$ . The LO curve is the  $p_T$  of either the  $Z$  or the  $b$  jet. At NLO, the distributions of both the  $Z$  and the highest- $p_T$   $b$  jet are shown for the inclusive cross section.

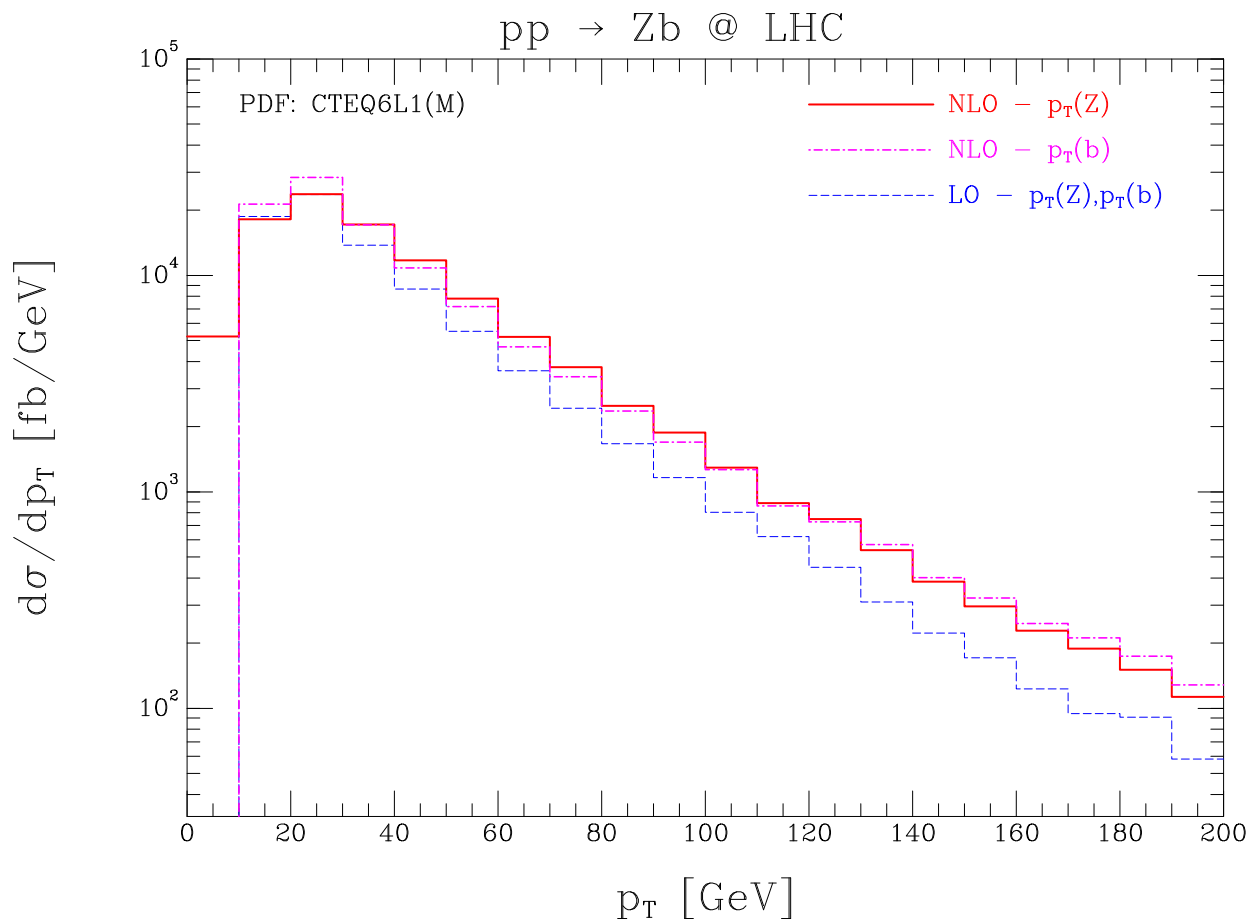


Figure 9: Same as Fig. 8, but at the LHC.